RESEARCH PAPER

Phosphoregulation in the N-terminus of NRT2.1 affects nitrate uptake by controlling the interaction of NRT2.1 with NAR2.1 and kinase HPCAL1 in Arabidopsis

Zhi Li[1,†], Xu Na Wu[1,‡], Aurore Jacquot[2], Valentin Chaput[2,iD], Mattia Adamo[2], Benjamin Neuhäuser[3,iD], Tatiana Straub[1], Laurence Lejay[2,iD], and Waltraud X. Schulze[1,*,iD]

[1] Department of Plant Systems Biology, University of Hohenheim, D-70593, Stuttgart, Germany
[2] BPMP, University Montpellier, CNRS, INRAE, Montpellier SupAgro, Montpellier, France
[3] Department of Crop Physiology, University of Hohenheim, D-70593, Stuttgart, Germany
[†] Present address: Department of Biology, University of North Carolina at Chapel Hill, Chapel Hill, NC 27599, USA.
[‡] Present address: State Key Laboratory of Conservation and Utilization of Bio-Resources in Yunnan and Center for Life Science, School of Life Sciences, Yunnan University, Kunming, China.

* Correspondence: wschulze@uni-hohenheim.de

Abstract

NRT2.1, the major high affinity nitrate transporter in roots, can be phosphorylated at five different sites within the N- and the C-terminus. Here, we characterized the functional relationship of two N-terminal phosphorylation sites, S21 and S28, in Arabidopsis. Based on a site-specific correlation network, we identified a receptor kinase (HPCAL1, AT5G49770), phosphorylating NRT2.1 at S21 and resulting in active nitrate uptake. HPCAL1 itself was regulated by phosphorylation at S839 and S870 within its kinase domain. In the active state, when S839 was dephosphorylated and S870 was phosphorylated, HPCAL1 was found to interact with the N-terminus of NRT2.1, mainly when S28 was dephosphorylated. Phosphorylation of NRT2.1 at S21 resulted in a reduced interaction of NRT2.1 with its activator NAR2.1, but nitrate transport activity remained. By contrast, phosphorylated NRT2.1 at S28 enhanced the interaction with NAR2.1, but reduced the interaction with HPCAL1. Here we identified HPCAL1 as the kinase affecting this phospho-switch through phosphorylation of NRT2.1 at S21.

Keywords: Kinase HPCAL1, nitrate, nitrate transporter NRT2.1, plasma membrane, post-translational regulation, protein phosphorylation.

Introduction

For most plants growing in temperate regions, nitrate is the main form of nitrogen taken up from the soil, which is mediated by members of the NRT2 and NPF protein families (Leran *et al.*, 2014). The uptake of nitrate through dedicated transporters has been under study for a long time (Krapp *et al.*, 2014), and several nitrate transporters in roots as well as in green tissue have been identified (Kiba *et al.*, 2012). These nitrate transporters are classified into two major groups based on

their uptake modes as a low affinity transport system (LATS) or a high affinity transport system (HATS) (Wang *et al.*, 2012).

NRT2.1 (AT1G08090) is the major high affinity nitrate transporter in Arabidopsis roots, as shown by the loss of 75% of HATS activity in *nrt2.1* knockout mutants (Cerezo *et al.*, 2001). A strong correlation between root nitrate influx and *NRT2.1* gene expression was observed (Lejay *et al.*, 1999; Girin *et al.*, 2007), leading to the conclusion that transcriptional regulation of NRT2.1 is a key mechanism to control nitrate uptake. Consequently, regulation of NRT2.1 in the past was mainly studied at the gene transcriptional level. *NRT2.1* gene expression is induced by nitrate (Lejay *et al.*, 1999) and repressed by high nitrogen metabolism and high external nitrate concentrations (Lejay *et al.*, 1999; Girin *et al.*, 2007). By contrast, *NRT2.1* gene expression was up-regulated by light and sugars (Lejay *et al.*, 1999, 2003) and is affected by the C/N status of the plant (Girin *et al.*, 2007; Krouk *et al.*, 2010). Further, reciprocal regulation of NRT2.1 and ammonium transporters by nitrate and ammonium influx was described (Gansel *et al.*, 2001; Camanes *et al.*, 2012).

NRT2.1 is regulated by protein–protein interaction with a small single transmembrane protein, NAR2.1 (AT5G50200) (Orsel *et al.*, 2007; Laugier *et al.*, 2012). Both proteins need to be present in the plasma membrane to result in full nitrate uptake activity (Orsel *et al.*, 2006). In addition, *nar2.1* mutants seem to be defective in trafficking of NRT2.1 to the plasma membrane (Wirth *et al.*, 2007). NAR2.1 was proposed to form a hetero-oligomer with NRT2.1 (Yong *et al.*, 2010), but the precise mechanism by which this complex forms remains unclear. Furthermore, the abundance of NRT2.1 protein within the membrane remains rather constant despite measurable changes in HATS activity upon stimulation by high nitrate, sugars, or light (Wirth *et al.*, 2007; Laugier *et al.*, 2012). This points to tight control of NRT2.1 activity by post-translational modifications. Post-translational control of nitrate transport activity is well described for the dual-affinity transporter NRT1.1 (AT1G12110) (Liu *et al.*, 1999; Guo *et al.*, 2001). In NRT1.1, phosphorylation at T01 acts as a switch. When T101 is phosphorylated, NRT1.1 functions as a high affinity transporter. When T101 is dephosphorylated, NRT1.1 functions as a low affinity transporter (Liu and Tsay, 2003). This affinity switch by phosphorylation has recently been related to conformational changes of NRT1.1 (Parker and Newstead, 2014). CIPK23 (AT1G30270) was identified as a kinase phosphorylating NRT1.1 at T101 (Ho *et al.*, 2009).

With accumulation of global (phospho)proteomics datasets acquired under nitrate stimulation (Engelsberger and Schulze, 2012; Wang *et al.*, 2013) or nitrate deprivation (Menz *et al.*, 2016), several phosphorylation sites for NRT2.1 were identified. However, the functional consequence of NRT2.1 N-terminal phosphorylation is as yet unclear, and the respective kinases and phosphatases remain uncharacterized. Here, we studied the NRT2.1 post-translational modification status under different conditions of nitrate availability. We aimed to identify kinases that might exert post-translational control of the major nitrate uptake transporter NRT2.1.

Materials and methods

Experimental design

Two phosphoproteomics datasets were used to study NRT2.1 phosphorylation and reconstruct kinase–substrate networks. Firstly, we used a previously published nitrate deprivation dataset (Supplementary Fig. S1A) in which plants were grown in hydroponic culture at 3 mM nitrate and then subjected to nitrate deprivation by transferring plants to nitrate-free nutrient solution. Plants were harvested before nitrate starvation (0 min), and after 15 min and 3 h of nitrate deprivation (Menz *et al.*, 2016). Secondly, we conducted a nitrate resupply experiment (Supplementary Fig. S1B), in which plants were grown at 3 mM nitrate, then starved for nitrate for 2 d. After starvation, nitrate was resupplied at a concentration of 0.2 mM or 5 mM for 5 min and 15 min. In all experiments, 3–4 biological replicates of root tissue were processed for (phospho)proteomic analysis and results are presented as averages with the SD. Statistical comparisons were carried out by pairwise *t*-tests (two sample comparisons) or one-way ANOVA (multiple sample comparisons).

Plant material

Experiments were performed with *Arabidopsis thaliana* wild type (Col-0) and the homozygous knockout mutants *nrt2.1* (SALK_035429) and *at5g49770* (SALK_068035) with T-DNA insertion in the promoter region. No AT5G49770 protein was detected in the knockout line.

Constructs

Constructs were made using Gateway technology. For ratiometric bimolecular fluorescence complementation (rBiFC) of Arabidopsis proteins, cDNAs of the following genes were cloned into rBiFC plasmids (Grefen and Blatt, 2012): AT5G49770 without and with phosphorylation site mutations at T792, S839, S870, and S919; and NRT2.1 without and with phosphorylation site mutations at S11, S21, and S28. Phosphorylation sites were mutated either to alanine (mimicking no phosphorylation) or to aspartate (putative phosphorylation mimic). For purification of the cytoplasmic domain of AT5G49770 to be used in *in vitro* kinase assays, the cytoplasmic domain (amino acids 583–946) was cloned into *Escherichia coli* BL21(DE3) expression plasmid pET-21a(+) and fused with a His-tag (plasmid AT5G49770CD-HIS). Cytoplasmic domains of two homologs, AT5G49760 (HPCA1/CARD1) and AT5G49780, were also used.

In vitro *kinase activity assay*

Plasmids expressing kinase domains with and without phosphorylation site mutations were transferred into *E. coli* BL21(DE3). After induction with isopropyl-β-D-thiogalactopyranoside (IPTG), cells were harvested and lysed using BugBuster Protein Extraction Reagent (Novagen, Nottingham, UK), and expressed proteins were purified over gravity flow Ni^{2+}-NTA Sepharose (IBA GmbH, Goettingen, Germany). *In vitro* kinase assays were performed using the ADP-Glo™Kinase assay kit (Promega, Germany) with minor modifications. Kinase (cytoplasmic domain, 1 nmol) was incubated with 5 μg of substrate in kinase reaction buffer (40 mM Tris–HCl, pH 7.5, 1 mM $MgCl_2$, 0.01% BSA, 50 μM NaF, 1 μM Na_3VO_3, 1 mM $CaCl_2$, 100 μM ATP, 1 mM DTT). As the generic kinase substrate, myelin basic protein was used in the kinase reaction buffer. After incubation for 1 h, 30 μl of ADP-GLO reagents (Promega, Germany) were added and incubated for 40 min. Then, kinase detection reagents were added and incubated for another hour. Luminescence as a measure

of ATP conversion from ADP was recorded with a luminometer (Tecan M200 Pro). Specific NRT2.1 substrate peptides were obtained from a QconCAT artificial protein consisting of concatenated tryptic peptides around NRT2.1 phosphorylation sites. After incubation at room temperature for 1 h, the reaction was terminated by heating at 90 °C for 10 min. Phosphopeptides were collected at the end of the kinase reaction over titanium dioxide.

Ratiometric bimolecular fluorescence assay

The rBiFC assays were conducted in transiently transformed *Nicotiana benthamiana* using a Zeiss LSM700 confocal microscope (X.N. Wu *et al.*, 2019). All images were collected using exactly the same settings. Yellow fluorescent protein (YFP) and red fluorescent protein (RFP) intensity was measured using the FIJI software (Schindelin *et al.*, 2012), and YFP/RFP ratios was calculated. From 10 to 50 different cells were analyzed. Statistical significance was determined using pairwise ranksum test. To calibrate YFP/RFP ratios, known interaction of NRT2.1 with NAR2.1 served as reference (Laugier *et al.*, 2012).

Nitrate influx assay

Root NO_3^- influx was assayed as described previously (Laugier *et al.*, 2012). Plants were sequentially transferred to 0.1 mM $CaSO_4$ for 1 min, to a complete nutrient solution, pH 5.8, containing 0.2 mM $^{15}NO_3$ (99 atom % excess^{15}N) for 5 min, and finally to 0.1 mM $CaSO_4$ for 1 min. Roots were then separated from shoots, and the roots dried at 70 °C for 48 h. After determination of their dry weight, samples were analyzed for total nitrogen and atom % ^{15}N using a continuous flow isotope ratio mass spectrometer coupled with a C/N elemental analyzer (ANCA-MS; PDZ Europa, Crewe, UK). Each influx value is the mean of 6–12 replicates.

Gene expression analysis

Root samples were frozen in liquid N_2 in 2 ml tubes containing one steel bead (2.5 mm diameter). Tissues were disrupted for 1 min at 28 s^{-1} in a mixer mill homogenizer (MM301, Retsch, Germany). Total RNA was extracted from tissues using Trizol reagent (Invitrogen, Carlsbad, CA, USA). Subsequently, 4 μg of RNA were treated with DNase I (Amplification Grade, Sigma–Aldrich) following the manufacturer's instructions. Reverse transcription was achieved with 4 μg of RNA in the presence of Moloney murine leukemia virus reverse transcriptase (RNase H minus, Point Mutant, Promega) after annealing with an anchored oligo(dT)$_{18}$ primer as described (Wirth *et al.*, 2007). The quality of the cDNA was verified by PCR using specific primers spanning an intron in gene APTR (At1g27450; see Supplementary Table S1).

Gene expression was determined by quantitative real-time PCR (LightCycler 480, Roche Diagnostics) using the SYBRR Premix Ex Taq^{TM} (TaKaRa) according to the manufacturer's instructions with 1 μl of cDNA in a total volume of 10 μl. All expression values were standardized to *Clathrin* (*At4g24550*). Gene-specific primer sequences are given in Supplementary Table S1. We selected the gene clathrin (At4g24550) as a control gene based on its lack of regulation by the conditions we are studying. It was independently identified as a suitable reference gene for nutrient experiments in a large-scale survey of 1400 possible reference genes across a wide range of conditions (Czechowski *et al.*, 2004).

Microsomal protein and phosphopeptide enrichment

A total of 1–1.5 g of root fresh weight was homogenized in 10 ml of ice-cold extraction buffer (330 mM mannitol, 100 mM KCl, 1 mM EDTA, 50 mM Tris-MES, fresh 5 mM DTT, and 1 mM PMSF, pH 7.5) (Pertl *et al.*, 2001) in the presence of 0.5% (v/v) proteinase inhibitor mixture (Sigma-Aldrich, Germany) and phosphatase inhibitors (25 mM NaF, 1 mM Na_3VO_4, 1 mM benzamidine, 3 μM proteinase inhibitor leupeptin). The homogenate was centrifuged for 15 min at 7500 *g* at 4 °C. The pellet was discarded, and the supernatant was centrifuged for 75 min at 48 000 *g* at 4 °C. Microsomal pellets were stored at −80 °C until further processing. Microsomal pellets were resuspended in 100 μl of membrane buffer (330 mM mannitol, 25 mM Tris-MES, 0.5 mM DTT) or UTU (6 M urea, 2 M thiourea, pH 8). Further tryptic digestion, desalting over C_{18}, and enrichment of phosphopeptides over titanium dioxide beads was performed as described (Wu *et al.*, 2017).

Liquid chromatograpy–tandem mass spectrometry analysis of peptides

Peptides mixtures were analyzed by a nanoflow Easy-nLC (Thermo Scientific) and a Orbitrap hybrid mass spectrometer (Q-Exactive, Thermo Scientific) as described previously (X.N. Wu *et al.*, 2019; Tan *et al.*, 2022). Proteins were identified based on information–dependent acquisition of fragmentation spectra of multiple charged peptides. MaxQuant version 1.5.3.8 (Cox and Mann, 2008) was used for raw file peak extraction and protein identification against the TAIR10 database (35 386 entries). Protein quantification was performed in MaxQuant using a label-free quantification algorithm (Cox *et al.*, 2014). The following parameters were applied: trypsin as cleaving enzyme; minimum peptide length of seven amino acids; maximal two missed cleavages; carbamidomethylation of cysteine as a fixed modification; and N-terminal protein acetylation and oxidation of methionine as variable modifications. For phosphopeptide identification, phosphorylations of serine, threonine, and tyrosine were included as variable modifications. Mass tolerances were used as in MaxQuant default settings: 4.5 ppm for precursor ions and 20 ppm as MS/MS tolerance. Further settings were: 'label-free quantification' marked, multiplicity set to 1; 'match between runs' marked with time window 0.7 min; peptide and protein false discovery rates (FDR) set to 0.01; and common contaminants (trypsin, keratin, etc.) excluded. The raw MS data from this study were deposited at the ProteomeXchange Consortium (http://proteomecentral.proteomexchange.org) via the PRIDE partner repository with the identifier PXD015390 for the nitrate starvation dataset and PXD014146 for the nitrate resupply dataset.

Statistical analyses and data visualization

Phosphosite ion intensity data were extracted from evidence.txt, $\log_2$–transformed, and normalized using Perseus (Tyanova *et al.*, 2016). Briefly, phosphosites quantified in at least 50% of the biological replicates were analyzed by ANOVA. Other statistical analyses were carried out with Sigma Plot (version 11.0) and Excel (version 2013). Over-representation analysis was done by Fisher's exact test; *P*-values were adjusted by Bonferroni correction. Functional classification of proteins was done based on MAPMAN (Thimm *et al.*, 2004). Information about subcellular location was derived from SUBA3 (Tanz *et al.*, 2013). Detailed protein function was manually updated with the support of TAIR (Huala *et al.*, 2001). Published protein–protein interactions were retrieved from STRING (Franceschini *et al.*, 2013).

Results

This work is based on two large-scale phosphoproteomics datasets of wild–type roots describing phosphorylation events induced by nitrate deprivation (Menz *et al.*, 2016) (Supplementary Fig. S1A) and nitrate resupply (Supplementary Fig. S1B). The MS raw data of these two experimental sets were jointly processed and quantified. In the combined dataset, 4746 phosphopeptides were identified (Supplementary Table S2), and at least

one quantitative value was obtained for 4670 phosphopeptides. Nitrate deprivation and nitrate resupply affected phosphorylation of diverse proteins at the plasma membrane, particularly the phosphorylation of H^+–ATPases (bin 34.1), and aquaporins (bin 34.19), which were down-regulated (dephosphorylated) by nitrate starvation and up-regulated (phosphorylated) by nitrate resupply. Proteins of protein synthesis (bin 29.2.1) and various signaling pathways through receptor kinases (bin 30.2) and calcium (bin 30.3) were also affected by both nitrate treatments. Proteins in glycolysis (bin 4.1) were only affected by nitrate deprivation (Supplementary Fig. S1C), while proteins of nitrate assimilation (bin 12.1.1) were increased in phosphorylation by nitrate resupply (Supplementary Fig. S1C).

NRT2.1 was found to be phosphorylated at different sites in the N- and the C-terminus, namely at S11 [(ac) GDSTGEPGSS(ph)MHGVTGR], S28 [EQSFAFSVQS(ph) PIVHTDK], S501 [NMHQGS(ph)LR], and T521 [SAAT(ph) PPENTPNNV], with distinct phosphopeptide intensities under nitrate starvation or nitrate resupply. Phosphorylation at S28 was quantified already in previous starvation–resupply experiments (Engelsberger and Schulze, 2012). The phosphopeptides corresponding to phosphorylation at S11, S28, S501, and T521 sites were also identified in independent nitrate nutrition experiments (Jacquot *et al.*, 2020). Phosphorylation at S21 with peptide EQS(ph)FAFSVQSPIVHTDK (Supplementary Fig. S2; Supplementary Table S2) has not been explicitly described previously, and was identified by careful re-analysis of nitrate deprivation datasets (Menz *et al.*, 2016).

NRT2.1 activity is regulated by N-terminal phosphorylation

To understand the role of N-terminal phosphorylation sites for the activity of NRT2.1, site-directed mutants of NRT2.1 were created, in which major phosphorylation sites were mutated to a putative phosphomimicking aspartate (D), or phosphodead alanine (A). These site-directed NRT2.1 mutants were expressed under the *NRT2.1* promoter in the *nrt2.1* knockout background. Nitrate influx was measured for nitrate-starved plants, as well as for plants after nitrate induction with 1 mM nitrate for 1 h and 4 h. In the wild type, higher nitrate influx was measured after 4 h of induction compared with nitrate influx rates of roots starved for nitrogen. In the *nrt2.1-2* knockout mutant, no induction of nitrate uptake was observed by 1 mM nitrate treatment, resulting in significantly lower nitrate uptake than in the wild type after 4 h of induction (Fig. 1). Phosphorylation site mutations at NRT2.1 S11 resulted in a wild-type-like influx of $^{15}NO_3^-$ under all conditions in the phosphodead S11A mutant, while nitrate influx was significantly reduced in phosphomimicking S11D mutants, although influx rates remained still higher than in the *nrt2.1* knockout mutant (Fig. 1A). This suggests that phosphorylation of NRT2.1 at S11 down-regulates nitrate influx. For phosphorylation site mutations at S28, we observed a significantly reduced nitrate

influx for S28A mutants similar to the *nrt2.1* knockout mutant, and wild-type-like nitrate influx for phosphomimicking mutation S28D (Fig. 1B). This suggests that phosphorylation of NRT2.1 at S28 activates nitrate influx directly or stabilizes NRT2.1 protein turnover. For newly discovered phosphorylation site S21, we also found reduced nitrate influx activity for plants with phosphodead S21A (Fig. 1C), while for plants with phosphomimicking S21D, averaged nitrate influx activity was higher than in plant lines with S21A after 4 h of 1 mM nitrate resupply. This suggests that phosphorylation at S21 also leads to a higher activity of NRT2.1.

Phosphorylation-dependent NRT2.1 regulation through interaction with NAR2.1

Nitrate transporter NRT2.1 is regulated by the interaction with protein NAR2.1 (Orsel *et al.*, 2006, 2007; Laugier *et al.*, 2012). Therefore, we used rBiFC (Grefen and Blatt, 2012) to explore whether the interaction of NRT2.1 with NAR2.1 was affected by NRT2.1 phosphorylation (Fig. 2A; Supplementary Fig. S3). The confirmed interaction of NRT2.1 with NAR2.1 was used as a reference. There was no difference between the phosphomimic mutation (S11D) and phosphodead mutations (S11A) for S11. For S21 we observed a significantly increased interaction of NAR2.1 with phosphodead S21A compared with the phosphomimicking S21D, which displayed a weaker interaction with NAR2.1. By contrast, NRT2.1 with phosphomimicking S28D displayed stronger interaction with NAR2.1 than NRT2.1 with phosphodead mutation S28A. Interestingly, however, if both phosphorylation sites were mutated together to create a mimic of a singly phosphorylated NRT2.1 N-terminus (S21A/S28D, S21D/S28A), NAR2.1 showed strong interactions with both versions and the highest interaction with the version phosphomimicking S28D. This suggests that a single phosphosite in the N-terminus is sufficient for interaction of NRT2.1 and NAR2.1, but S28 is the preferred site. Since the *in vivo* phosphorylation status of NRT2.1 in singly mutated constructs (Fig. 2A) remains unknown, the doubly phospho-mutated version (Fig. 2B) gives more precise insights.

Identification of kinases phosphorylating NRT2.1

Based on existing nitrate starvation and nitrate resupply datasets (Engelsberger and Schulze, 2012; Menz *et al.*, 2016), and with addition of data from new resupply experiments with 0.2 mM and 5 mM nitrate, we aimed to identify kinases acting on the different phosphorylation sites of NRT2.1. Many kinases are subject to regulation by phosphorylation (Zulawski and Schulze, 2015), suggesting that kinases phosphorylating NRT2.1 are likely also to be regulated by nitrate-dependent phosphorylation. Thus, we expected phosphorylation profiles of a kinase and its substrate to be highly correlated under conditions when phosphorylation of kinase and substrates both
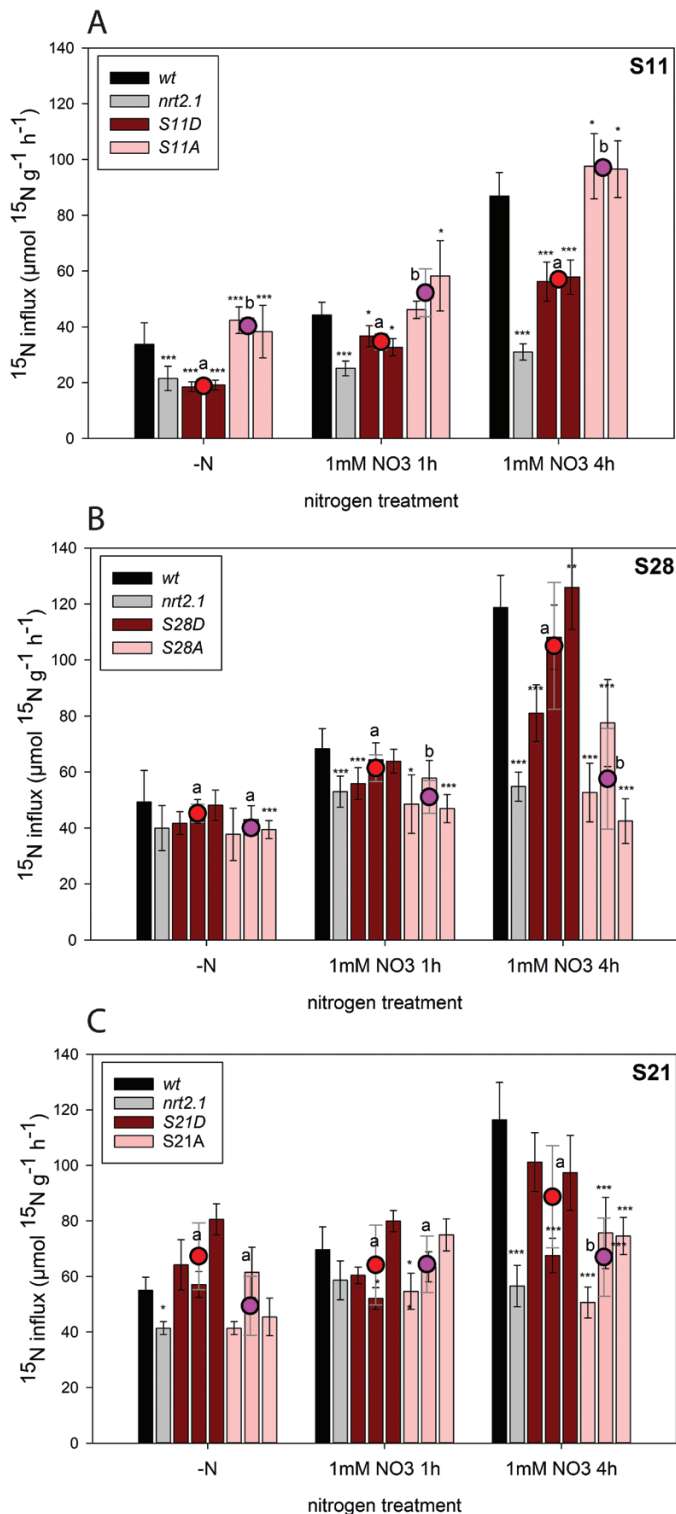
Fig. 1. Regulation of nitrate uptake by N-terminal NRT2.1 phosphorylation at (A) S11, (B) S28, and (C) S21. In all panels, the wild type and *nrt2.1* knockout mutant were used as controls. Phosphorylation site mutants of *NRT2.1* were expressed under the *NRT2.1* promoter in the *nrt2.1* mutant background as phosphomimicking (S to D) or phosphodead (S to A) versions of different phosphorylation sites. Bars of the same color indicate

independent lines expressing the same construct (S to D, or S to A). Averages with SD are displayed; asterisks indicate significant differences from the wild type within one treatment (***P<0.001, **P<0.01, *P<0.05, pairwise *t*-test). Dots indicate average uptake rates of different plant lines expressing S to D or S to A mutants. Letters indicate significant differences (*P*<0.05, pairwise *t*-test) between phosphomimicking and phosphodead mutants within each treatment.

have activating, or both have inactivating, effects. Alternatively, phosphorylation of a kinase and its substrates is expected to be anti-correlated if one activating and one inactivating phosphorylation occurs. To identify such kinase candidates, phosphorylation profiles of NRT2.1 phosphorylation sites S11, S28, S501, and T521 were correlated with phosphorylation profiles of identified kinases (Supplementary Fig. S4; Supplementary Table S3). NRT2.1 phosphorylation site S21 was not included due to low data coverage across conditions. Following this approach, phosphorylation profile correlation pairs were strictly filtered based on their correlation *r*-value (*r*>0.9 or *r*<−0.9). As a result, 12 protein kinases were identified only under nitrate deprivation, 30 protein kinases were identified only under nitrate resupply conditions (5 mM NO_3 or 0.2 mM NO_3), and nine protein kinases were identified under nitrate depletion as well as under nitrate resupply (Fig. 3A; Supplementary Table S3).

Kinases with phosphorylation profiles highly correlated with NRT2.1 phosphorylation included MAPKKK7 (AT3G13530), for which phosphorylation positively correlated with phosphorylation of NRT2.1 at S11 and T521. Phosphorylation of CIPK25 (AT5G25110) correlated with NRT2.1 phosphorylation at S11, and phosphorylation of calcium-dependent protein kinase 29 (CPK29, AT1G76040) was correlated with phosphorylation at T521. Phosphorylation of CDPK19 (AT5G19450) and MAP4K4 (AT5G14720) at different sites were connected to the phosphorylation profiles of NRT2.1 at S11, S28, and S501. Among the receptor kinases, phosphorylation of BAM1 (AT5G65700) positively correlated with S11 and S501 phosphorylation, and phosphorylation of phytosulfokine receptor 1 (PSKR1, AT2G02220) correlated with NRT2.1 phosphorylation at S501. C-terminal phosphorylation at LIEEVSHSSGS(ph)PNPVS(ph)D of co-receptor QSK1 (AT3G02880) showed a negative correlation with phosphorylation at S28 and T521. Phosphorylation of kinase AT5G49770 at S839 showed positive correlation with NRT2.1 phosphorylation at S28 under low nitrate supply (Supplementary Table S3). Receptor kinase AT5G49770 raised our further interest, since four phosphorylation sites were identified within the activation loop at T792 [LVGDPEKAHVT(ph)TQVK], in the kinase domain at S839 [SPIDRGS(ph)YVVK] and S870 [NLYDLQELLDTTIIQNS(ph)GNLKGFEK], and within the disordered C-terminal region at S919 [LVGLNPNADS(ph)ATYEEASGDPYGR] (Supplementary Fig. S5).

The phosphorylation network was further complemented with known interaction partners of NRT2.1 and
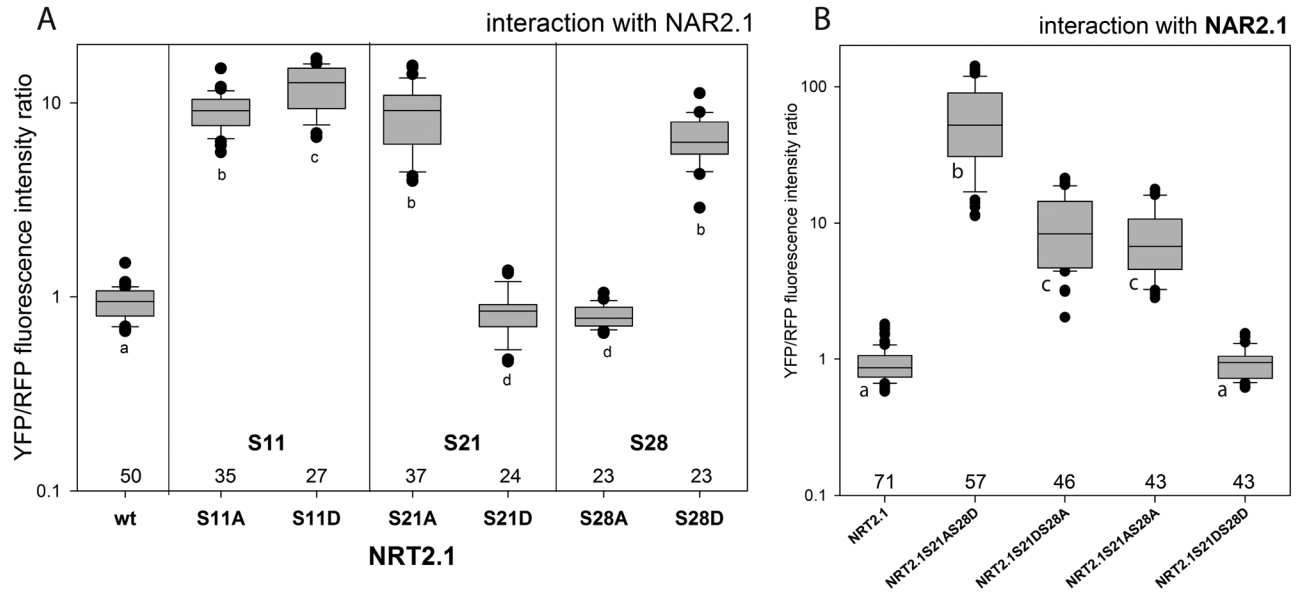
Fig. 2. Interaction of NRT2.1 with NAR2.1. (A) The effect of phosphodead (S to A) and phosphomimicking (S to D) mutations of NRT2.1 single phosphorylation site mutations on the interaction with NAR2.1. (B) The effect of double phosphorylation site mutations at S21 and S28 on the interaction with NAR2.1. Numbers indicate the total number of cells quantified. Lowercase letters indicate significant differences as determined by pairwise rank sum test (*P*<0.05). Higher YFP/RFP ratios indicate stronger interaction.

kinase candidate AT5G49770 as retrieved from public sources (Franceschini *et al.*, 2013) (Fig. 3B). Thereby, it became obvious that NRT2.1 was shown to interact with several other kinases besides AT5G49770, among them VIK1 (AT1G14000) (Wingenter *et al.*, 2011), a mitogen–activated protein (MAP) kinase (AT3G46930), phytosulfokine receptor kinase PSKR1 (AT2G02220), and several uncharacterized receptor kinases (Fig. 3B). By contrast, kinase AT5G49770 had been found to interact with various other transport proteins within the membrane besides NRT2.1, for example with H$^+$–ATPases AHA1 (AT2G18960) and AHA2 (AT4G30190), and several members of the ABC transporter family (PGP6 AT2G39480, PGP19 AT3G28860, PDR7 AT1G15210, PGP4 AT2G47000, PGP11 AT1G02520, MRP10 AT3G62700, and PGP20 AT3G55320). Furthermore, kinase AT5G49770 was connected to the calcium signaling pathway through interactions with CPK29 (AT1G76040), CPK7 (AT5G12480), CPK6 (AT2G17290), and CBL3 (AT4G26570). A connection to nitrate assimilation was found through interaction of AT5G49770 with nitrate reductases NIA2 (AT1G37130) and NIA1 (AT1G77760).

Kinase AT5G49770 interacts with and phosphorylates NRT2.1

Kinase candidate AT5G49770 was then tested for its ability to interact with NRT2.1 *in planta*, and we further tested whether this interaction was affected by the phosphorylation status of the kinase. Indeed, we showed an interaction of AT5G49770 with NRT2.1 in the rBiFC system (Fig. 4A; Supplementary Fig. S6A). Phosphorylation site mutations of AT5G49770 at

sites T792, S870, and S919 did not affect the interaction with NRT2.1. However, when S839 was mutated to alanine, interaction of AT5G49770 S839A with NRT2.1 was significantly increased compared with AT5G49770 S839D, when S839 was mutated to phosphomimicking aspartate. Thus, interaction of AT5G49770 with NRT2.1 was stronger when S839 was dephosphorylated. Next, we explored NRT2.1 as a substrate for kinase AT5G49770 (Fig. 4B). The intracellular domain of AT5G49770 was recombinantly expressed (Supplementary Fig. S7) and exposed to the substrate peptide EQSFAFSVQSPIVHTDK in *in vitro* kinase assays (Wu and Schulze, 2015). Indeed, the kinase domain of AT5G49770 was able to phosphorylate the substrate peptide at S21. Significantly higher NRT2.1 S21 phosphorylation was observed from kinase domains with a phosphodead mutation S839A. By contrast, phosphomimicking mutation S839D yielded lower substrate phosphorylation at NRT2.1 S21 compared with AT5G49770S839A, but still higher kinase activities than in the wild type. Also, mutations at S870 lead to differential substrate phosphorylation efficiency: phosphomimicking mutation AT5G49770S870D resulted in higher kinase activity towards NRT2.1 N-terminal peptide than phosphodead mutation AT5G49770S870A. No significant differences in substrate phosphorylation between phosphomimicking and phosphodead versions of recombinant kinase domain were observed for other phosphorylation sites in AT5G49770 (Fig. 4B). Consistently, all *in vitro* kinase activity assays showed substrate phosphorylation only at the serine corresponding to NRT2.1 S21 (Fig. 4C), and never at the site corresponding to S28 or the double phosphorylated forms.
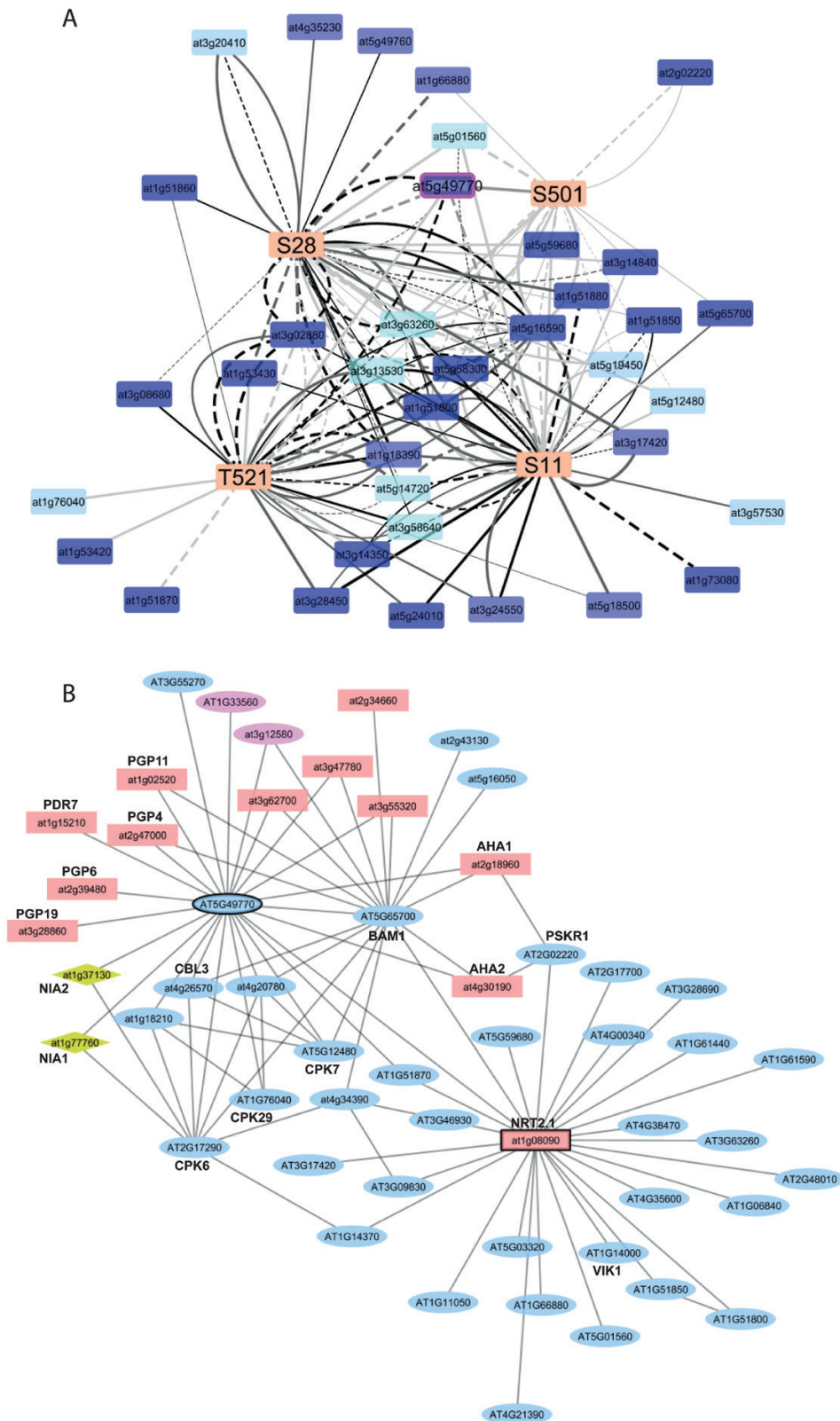
Fig. 3. Phosphorylation and interaction network of NRT2.1 and its putative kinases. (A) Correlation network of NRT2.1 phosphorylation sites S11, S28, S501, and T521 with plasma membrane-located kinases under nitrate deprivation and nitrate resupply with 5 mM and 0.2 mM NO_3^-. Solid edges, positive correlation; dashed edges, negative correlation. Edge color: black, 5 mM NO_3^-; gray, 0.2 mM NO_3^-; light gray, nitrogen deprivation. Node color: blue, receptor kinases; light blue, calcium signaling; gray, other kinases. (B) Interaction network of NRT2.1 and the selected putative kinase AT5G49770 extended by known experimentally confirmed interaction partners from STRING (Franceschini *et al.*, 2013). Node color: red, transport proteins; blue, signaling proteins; yellow, nitrogen metabolism; pink, other.

Interestingly, when the generic kinase substrate myelin basic protein was used in the *in vitro* kinase assay instead of specific NRT2.1 substrate peptide, phosphorylation site mutations at S839 did not result in differential kinase activity, and increased kinase activity was only observed for the AT5G49770S870D mutation (Fig. 4D). These results suggest that phosphorylation of AT5G49770 at S870 regulated general kinase activity (towards a generic substrate), while phosphorylation of AT5G49770 at S839 rather affected interaction with the specific substrate. Indeed, when S839 was phosphorylated (phosphomimicked S839D), interaction of AT5G49770 with NRT2.1 was reduced (Fig. 4A) and lower levels of substrate phosphorylation at S21 occurred (Fig. 4B). When S870 was phosphorylated (phosphomimicked S870D), kinase activity

generally was enhanced (Fig. 4D), there was higher phosphorylation activity towards the NRT2.1 S21 peptide, but overall interaction of AT5G49770 with NRT2.1 was not significantly affected (Fig. 4A).

We then checked the *in planta* phosphorylation status of NRT2.1 and AT5G49770 (Fig. 5) in the two nitrogen nutrition experiments, namely nitrogen deprivation for 15 min and 3 h (Menz *et al.*, 2016), and nitrate starvation resupply experiment with 2 d of nitrate starvation followed by resupply of either 0.2 mM or 5 mM nitrate for 5 min or 15 min. NRT2.1 S21 tended to be increasingly phosphorylated at nitrate resupply with high (5 mM) nitrate, but not under prolonged nitrate starvation for 2 d (Fig. 5A). By contrast, NRT2.1 S28 was phosphorylated under nitrate starvation and low nitrate supply,
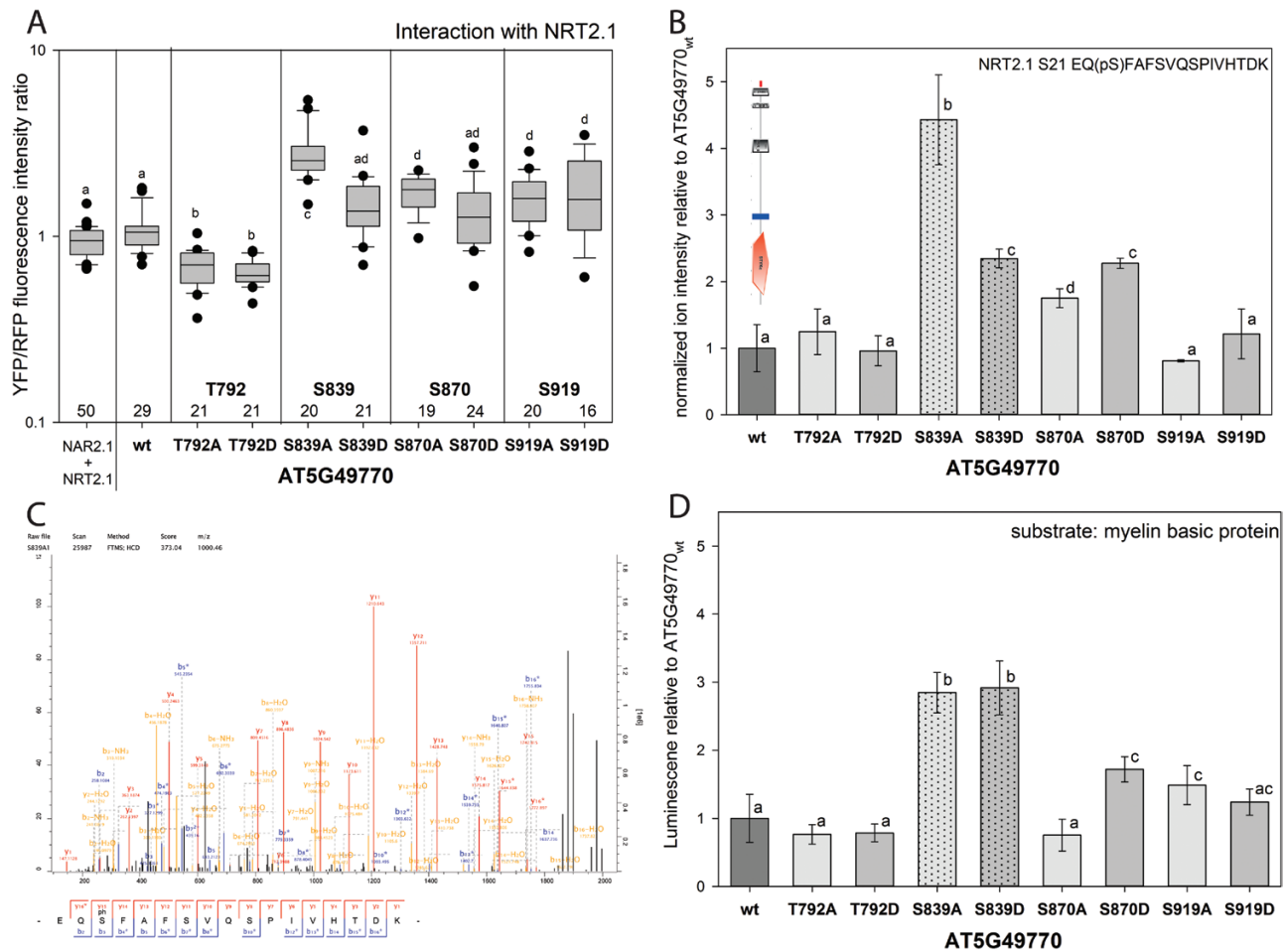
Fig. 4. Kinase AT5G49770 interacts with and phosphorylates NRT2.1 at S21. (A) The effect of phosphodead (S to A) and phosphomimicking (S to D) mutations of AT5G49770 phosphorylation sites on the interaction with NRT2.1. Numbers indicate the total number of cells quantified. Lowercase letters indicate significant differences as determined by pairwise rank sum test ($P<0.05$). (B) *In vitro* kinase activity assay using the NRT2.1 peptide EQSFAFSVQSPIVHTDK as a substrate. Averages with SDs are displayed; lowercase letters indicate significant differences based on pairwise t-test ($P<0.05$). Dotted bars denote phosphorylation site S839. A domain model of the AT5G49770 kinase based on SMART is displayed as an insert (Schultz *et al.*, 1998). (C) Representative fragment spectrum of *in vitro* kinase activity assay showing specific phosphorylation of the substrate peptide EQSFAFSVQSPIVHTDK at S21. The spectrum was directly exported from MaxQuant version 1.5.3.30 (Cox and Mann, 2008). (D) *In vitro* kinase activity assay using myelin basic protein as a substrate. Averages with SDs are displayed; lowercase letters indicate significant differences based on pairwise t-test ($P<0.05$).

and showed a trend for dephosphorylation at high nitrate concentrations (5 mM) (Fig. 5B). This confirmed published observations of NRT2.1 S28 dephosphorylation upon 3 mM nitrate resupply (Engelsberger and Schulze, 2012). Kinase AT5G49770 was found with increased phosphorylation at S870 after resupply of 5 mM nitrate (Fig. 5C) and a decreased phosphorylation at S839 under these conditions (Fig. 5D). Other phosphorylation sites of AT5G49770 were only detected at very low levels under nitrogen starvation and resupply with low (0.2 mM) nitrate (Fig. 5E). In summary, NRT2.1 phosphorylation at S21 and S28 showed a tendency for anti-correlation at high nitrate supply: when S21 was highly phosphorylated, phosphorylation at S28 was detected at a lower level and vice versa (Fig. 5A, B). A similar anti-correlation was also observed for S839 and S870 of kinase AT5G49770 (Fig. 5C, D).

Nitrate uptake in kinase mutant at5g49770

Interaction of kinase AT5G49770 with NRT2.1 in BiFC assays was found to be affected by NRT2.1 phosphorylation status at S28 (Fig. 5F; Supplementary Fig. S6B). AT5G49770 showed significantly weaker interactions with NRT2.1 in the phosphorylation-mimicking NRT2.1S28D mutant compared with phosphodead NRT2.1S28A. This suggests that interaction of kinase AT5G49770 with NRT2.1 is not favored by phosphorylation at S28 (Fig. 5F). Testing the interaction of AT5G49770 with the double-mutated NRT2.1 confirmed reduced interaction of the kinase with NRT2.1 S28D and stronger interaction of the kinase with the NRT2.1 S21D (Supplementary Fig. S6C). The interaction of AT5G49770 with NRT2.1 mutated at S11 remained largely unaffected (Fig. 5F).

In the knockout mutant *at5G49770*, we observed a significantly higher nitrate influx than in the *nrt2.1* knockout (Fig. 6A), reaching wild-type-like nitrate influx rates upon nitrate induction (1 mM NO_3^- for 4 h or 7 h). Thus, in the absence of AT5G49770, nitrate influx was high, consistent with high activity of NRT2.1. We therefore propose that under 1 mM nitrate supply, in the absence of AT5G49770, NRT2.1 may remain in the highly active complex together with NAR2.1 when S28 is phosphorylated. The active state observed when AT5G49770 showed the highest interaction with NRT2.1, namely when S28 is dephosphorylated, may occur under specific cellular conditions. It may not be the dominant state of NRT2.1 and could be a transition state to fine-tune NRT2.1 activity status. Kinase AT5G49770 was recently named HPCAL1, as a homolog of H_2O_2 receptor HPCA1 (Wu *et al.*, 2020) and/or as a quinone receptor CARD1 (Laohavisit *et al.*, 2020). The observed uptake rates in the *hpcal1* (*at5g49770*) knockout mutant were consistent with unaltered *NRT2.1* mRNA abundance in the mutant (Fig. 6B). However, a reduced expression of *NAR2.1* mRNA was observed in the kinase mutant *at5g49770* (Fig. 6B), suggesting the possibility of downstream signaling effects. Expression of *AT5g49770* was not dependent on the presence of NRT2.1, since the

nrt2.1 mutant showed similar levels of *Hpcal1* (*At5g49770*) mRNA to the wild type, at least under the conditions tested here (Fig. 6B).

Since phosphorylation of NRT2.1 at S28 was also shown to affect NRT2.1 stability (Zou *et al.*, 2019), we analyzed NRT2.1 protein abundance under conditions of 4 h nitrate induction used for nitrate influx assays. The abundance of NRT2.1 was significantly reduced in transgenic plants bearing phosphodead NRT2.1S28A (Supplementary Fig. S8A). This confirms stabilization of NRT2.1 by phosphorylation at S28 (Zou *et al.*, 2019). The protein abundance of NAR2.1 (Supplementary Fig. S8B) as well as that of kinase HPLCAL1 (Supplementary Fig. S8C) were not affected by phosphorylation site mutations of NRT2.1 at S21 or S28.

Discussion

There are (at least) five phosphorylation sites which differentially affect nitrate uptake of nitrate transporter NRT2.1. In the C-terminus, phosphorylation of S501 was recently shown to result in inactivation of NRT2.1 without affecting the interaction of NRT2.1 with NAR2.1 (Jacquot *et al.*, 2020). In the N-terminus, phosphorylation (or phosphomimic) of S28 mediated high nitrate uptake, while phosphorylation at S11 resulted in low nitrate uptake. Phosphorylation at S28 was shown to stabilize NRT2.1 at the plasma membrane (Zou *et al.*, 2019), but may additionally lead to direct regulation by affecting interactions with NAR2.1. The molecular mechanisms by which this post-translational control at these different sites takes effect can be very different for each of these sites. Interestingly, dephosphorylation at S11 enhanced NRT2.1 transport activity, but interaction with NAR2.1 was not affected by the phosphorylation state at S11. This indicates that transport activity of NRT2.1 may require further regulation even when NRT2.1 interacted with NAR2.1. The main discovery in our study is that single phosphorylation of NRT2.1 at either S21 or S28 results in active nitrate influx, and that HCAL1 is the kinase involved in NRT2.1 phosphorylation at S21. Interestingly, kinase HPCAL1 was also proposed to interact with nitrate transporters (also NRT1.1) in a size-exclusion chromatography coupled to MS approach, separating protein complexes and reconstructing their interaction network (Gilbert and Schulze, 2019; Gilbert *et al.*, 2021).

It is well known that phosphorylation of the same protein at different sites, or different modifications at closely neighboring sites, can influence the nature of protein–protein interactions and consequently the activity of proteins or signaling pathways. Recently, in plant receptor kinase signaling, a tyrosine phosphorylation switch has been discovered in BAK1/SERK3 which in the phosphorylated state activates immune signaling, and in the dephosphorylated state feeds into other signaling pathways (Perraki *et al.*, 2018). Also, multisite phosphorylation in ribosomal protein S6 kinase 1 (S6K1) was
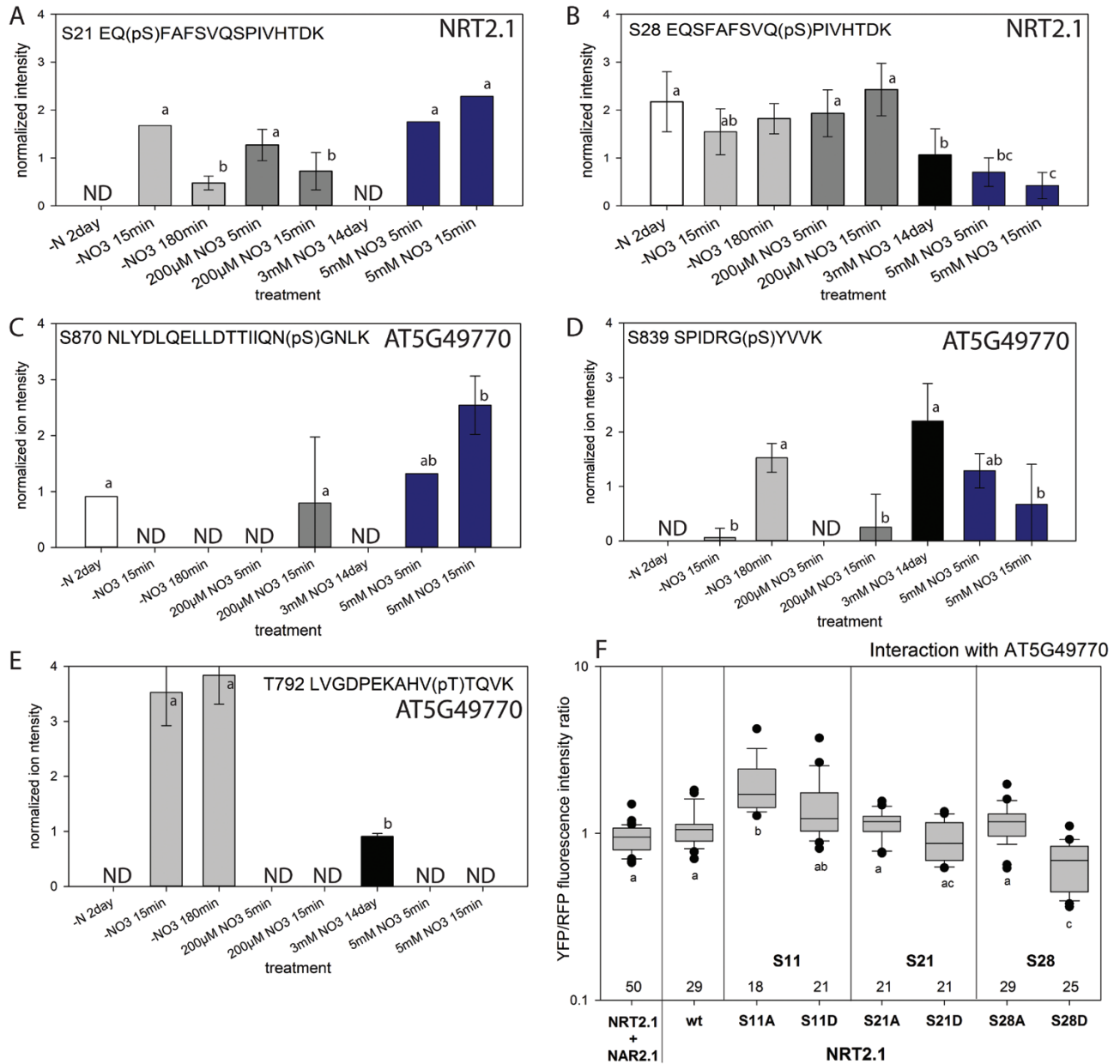
Fig. 5. Phosphorylation status of NRT2.1 S21, S28, and AT5G49770 S870, S839 under different nutritional contexts. Results show the abundance of individual phosphopeptides and cannot confirm phosphorylation combinations of individual NRT2.1 molecules. (A) Phosphorylation of NRT2.1 at S21. (B) Phosphorylation of NRT2.1 at S28. (C) Phosphorylation of AT5G49770 at S870. (D) Phosphorylation of AT5G49770 at S839. In (A–D), raw files from previous experiments (Engelsberger and Schulze, 2012; Menz *et al.*, 2016) and current experiment of resupply with 0.2 mM and 5 mM nitrate were processed together and quantified. Average normalized ion intensity values of three biological replicates are shown with SD as determined by cRacker (Zauber and Schulze, 2012). ND: not detected. (E) Interaction of AT5G49770 with NRT2.1 and respective NRT2.1 phosphorylation site mutants as determined from rBiFC experiments. Numbers indicate the number of quantified cells. In all panels, lowercase letters indicate significant differences as derived from a one-way ANOVA ($P<0.05$).

shown to alter substrate specificity of the kinase (Arif *et al.*, 2018). Phosphorylation of three different sites at S6K1 was required for it to phosphorylate one substrate but not the other. Here, we present an example in which phosphorylation at spatially closely neighboring serine residues in the N-terminus of NRT2.1 resulted in preferred recruitment of different interaction partners, either NAR2.1 or kinase HPCAL1, to these particular sites. Currently, it cannot be excluded that trimeric complexes exist, and it is also likely that the interaction status of individual NRT2.1 molecules could be in different interaction states, leading to a mixture of complexes. Nitrogen status and the resulting phosphorylation status of NRT2.1
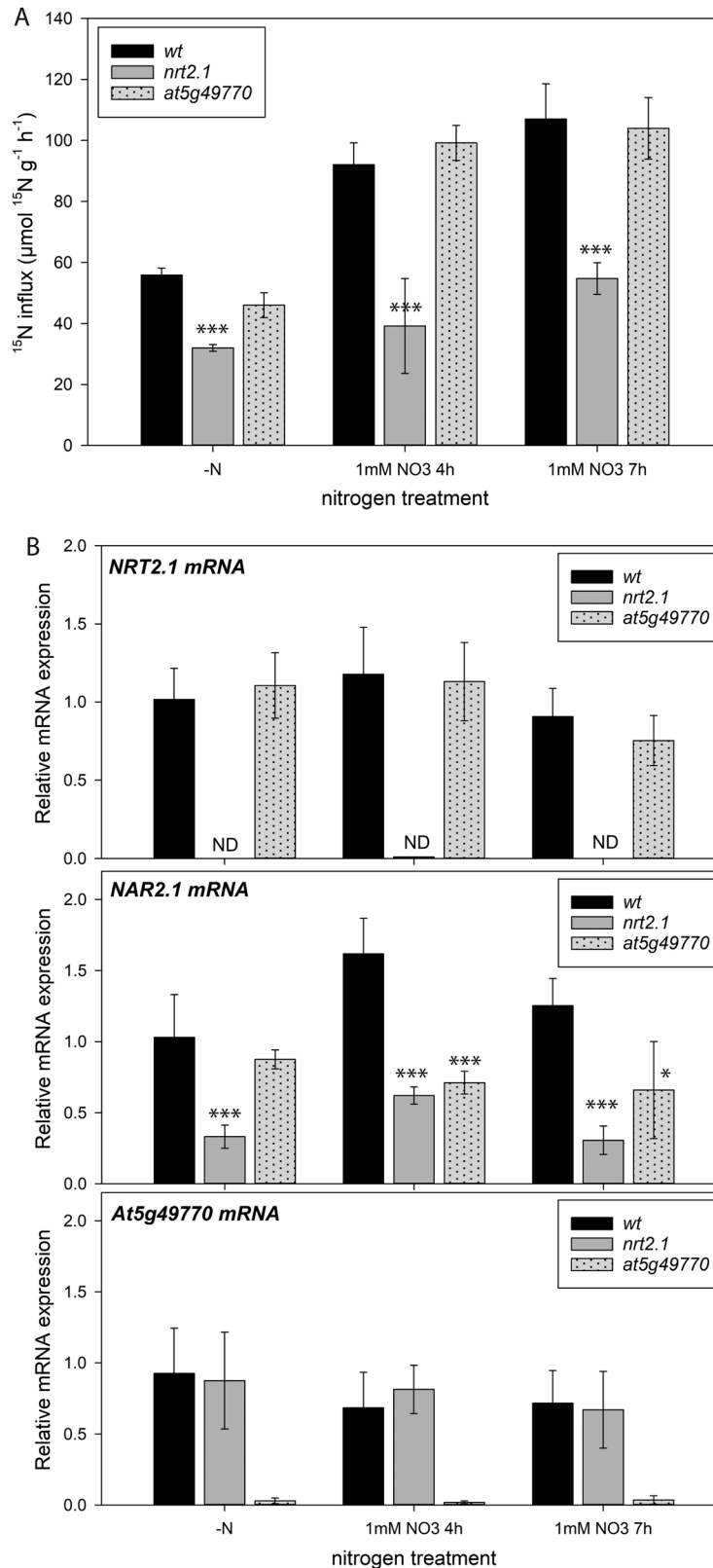
Fig. 6. Interaction of AT5G49770 with NRT2.1 phosphorylation site mutants and nitrate uptake of a kinase knockout. (A) Nitrate influx rate of the wild type, *nrt2.1* knockout, and *at5g49770* knockout under nitrate starvation (–N) and induction with 1 mM nitrate for 4 h and 7 h. Averages (*n*=4) with SDs are shown. (B) Expression of *NRT2.1*, (C) *NAR2.1* mRNA, and (D) *At5g49770* mRNA in the wild type, *nrt2.1* knockout, and *at5g49770* knockout mutant. Averages of three biological replicates are shown with SD; asterisks indicate significant differences from the wild type within one treatment (***$P<0.001$, **$P<0.01$, *$P<0.05$, pairwise *t*-test).

probably determine the dominant complex form of NRT2.1 and thus the resulting uptake rates.

Regulation of transporters at the plasma membrane by multiple phosphorylation sites, as described here for NRT2.1, could well be a general principle, particularly for proteins that are under control of many different signals. For example, the H^+-ATPase AHA2 is regulated by two different activating phosphorylation sites in its C-terminus and by at least one inactivating phosphorylation site in one cytosolic loop (Rudashevskaya *et al.*, 2012). In addition, these regulatory phosphorylation sites of AHA2 are targeted by different kinases which control proton flux in response to different stimuli (Fuglsang *et al.*, 2003, 2014; Haruta *et al.*, 2008, 2015; Caesar *et al.*, 2011). A role in fine-tuning of transporter activity was recently also proposed for a series of serine phosphorylation sites in the C-terminus of the ammonium transporter family (X. Wu *et al.*, 2019).

Functional model of the NRT2.1 phosphoregulation at S21/S28

NRT2.1 here was found to be phosphorylated with several sites at the N- and the C-terminus. At the same time, the regulatory pattern of NRT2.1 turned out to be very complex and under transcriptional and post-transcriptional control of external nitrate supply as well as the metabolic C/N status of the plant (Gansel *et al.*, 2001; Wirth *et al.*, 2007; Camanes *et al.*, 2012; Li *et al.*, 2016). Therefore, it is no surprise to find highly complex regulatory mechanisms involving phosphorylation sites in the N-terminus to add to the multifactorial control of NRT2.1 activity at the protein level. NRT2.1 is active mainly under low nitrate conditions (e.g. 0.2–1 mM). Under these conditions, NRT2.1 was found to be highly phosphorylated at S28 and showed strong interactions with activator NAR2.1 (Fig. 7A). Under low nitrate, HPCAL1 was found to be phosphorylated at S839, and in this state shows reduced interaction with NRT2.1. Most probably, HPCAL1 under these conditions is dephosphorylated at S870, corresponding to a less active kinase domain (Fig. 5C, D).

Under resupply of higher external nitrate (3–5 mM), NRT2.1 phosphorylation at S28 was reduced. This results in decreased protein stability (Zou *et al.*, 2019), but also slightly enhances the interaction with receptor kinase HPCAL1 (Fig. 2). HPCAL1—dephosphorylated at S839 and activated by (auto)phosphorylation at S870 (Fig. 5)—can then interact with and phosphorylate NRT2.1 at S21 and switch it into an active state (Fig. 7B). In this active state NRT2.1 can still interact with NAR2.1 (Fig. 2B).

The double-phosphorylated state of NRT2.1 (Supplementary Fig. S9) was experimentally only found transiently after nitrate resupply. In this state (Fig. 7C), the interaction with activator NAR2.1 was found to be weak (Fig. 2B), and uptake rates were lower (Supplementary Fig. S10). It could possibly present a fast mechanism to (temporarily) reduce nitrate influx. Such a (temporary) reduction in nitrate influx could be useful for the plant under limiting carbon availability and/or when sufficient amino acids have been built in the assimilation pathway (Lejay *et al.*, 1999; Girin *et al.*, 2010). The doubly dephosphorylated state (Fig. 7D) is considered as unstable at the plasma membrane (Supplementary Fig. S8A; Zou *et al.*, 2019) and may thus have a higher turnover. However, interaction of NRT2.1S21AS28A with activator NAR2.1 potentially remained (Fig. 2B). Our findings point to a significant regulation of NRT2.1 activity through phosphorylation events at S21 and S28. It needs to be kept in mind, however, that phosphoregulation of NRT2.1 at the C-terminus (Jacquot *et al.*, 2020) may add to the effects described here.

We suggest kinase HPCAL1 to function in switching unstable, double-dephosphorylated NRT2.1 to an active state by phosphorylation of S21 (Fig. 7D). In addition, HPCAL1 could also participate in switching NRT2.1 to the more inactive, double-phosphorylated state. When kinase HPCAL1 is absent (in *at5g49770*), NRT2.1 most probably remains stabilized in a highly active state phosphorylated at S28 (Fig. 7A) and in interaction with NAR2.1.

In support of our regulatory model, singly phosphorylated NRT2.1 (S21AS28D or S21DS28A) showed higher nitrate influx activity than double-dephosphorylated NRT2.1 (S21AS28A) or double-phosphorylated NRT2.1 (S21DS28D) (Supplementary Fig. S10). Activation of NRT2.1 was recently described to involve a type 2C protein phosphatase (Ohkubo *et al.*, 2021). Although in that study the action of the phosphatase dephosphorylated NRT2.1 at S501, we expect as yet unknown phosphatases to be involved in regulation of NRT2.1 also at the N-terminus.

Phosphoregulation of kinase HPCAL1

Receptor kinase HPCAL1 is highly and almost exclusively expressed in root tissue, particularly in the lateral root cap (Winter *et al.*, 2007), and shows high overlap with NRT2.1 expression. There are two closely related kinases (HPCA1/CARD1, AT5G49760; and HPCAL2, AT5G49780) within the Arabidopsis proteome sharing high homology with our candidate kinase AT5G49770 (Supplementary Fig. S10). AT5G49760 was highly expressed in leaf tissue and anthers, with rather low expression values in roots, and AT5G49780 showed moderate general expression also in roots, but at lower levels than AT5G49770 (Winter *et al.*, 2007). The phosphorylation site at S839 was unique to AT5G49770, while in AT5G49760 and AT5G49780 a lysine is present at the respective position within the sequence (Supplementary Fig. S10). In the kinase activity assays, AT5G49780 was largely inactive, while AT5G497760 (HPCA1/CARD1) displayed a higher activity towards substrate peptide EQSFAFSVQSPIVHTDK than did AT5G49770. This high activity could possibly be explained by the fact that the regulatory phosphorylation site identified for AT5G49770 with S839 was not present in AT5G49760 and therefore this kinase may show constitutively higher activity. We cannot provide a clear explanation for the observed
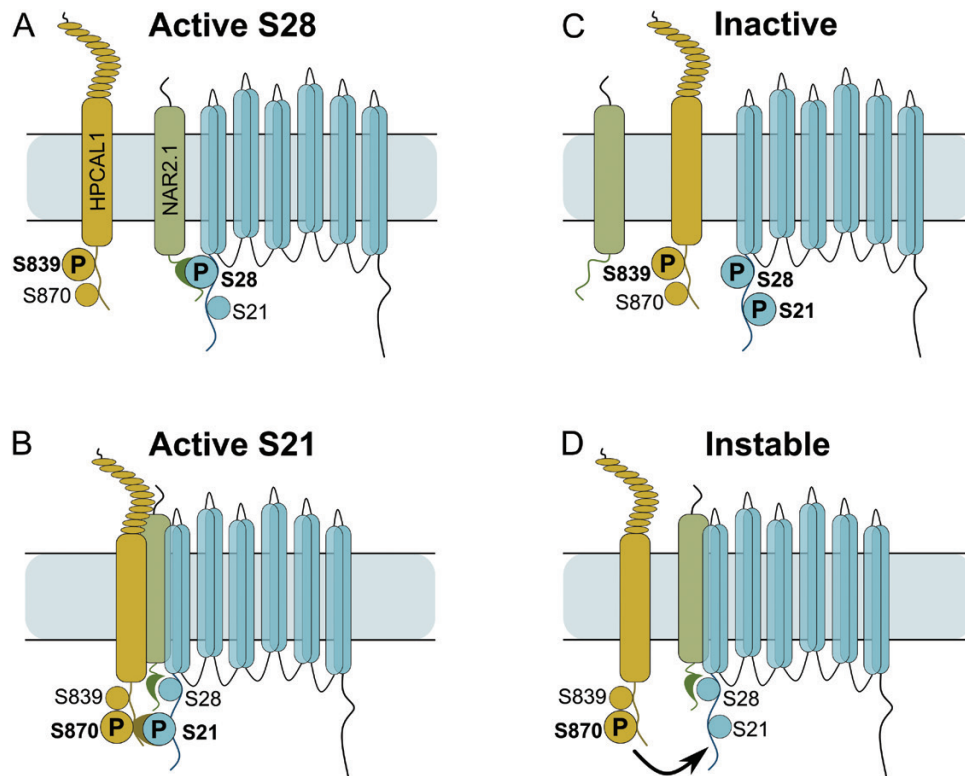
Fig. 7. Functional model of NRT2.1 regulation at the N-terminus involving two single phosphorylated states of NRT2.1 at S21 and S28 under conditions of induction by 1 mM nitrate for 4 h. NAR2.1 is shown in green and kinase HPCAL1 is shown in yellow. The functional relevance of other N- and C-terminal NRT2.1 phosphorylation sites was not considered in this figure.

inactivity of the recombinant kinase domain AT5G49780, but possibly this is connected to an additional sequence at amino acids 609–629 (Supplementary Fig. S10). Despite the orthologs, our proteomic evidence and gene expression patterns (Winter *et al.*, 2007) point to AT5G49770 (HPCAL1) as the dominant isoform in young root tissue which was analyzed here. The expression of AT5G49760 was dominant in leaves.

Protein kinases can be regulated by phosphorylation within their kinase domain. Most prominent examples are MAP kinases, which are activated by double-phosphorylation of a well-conserved TEY motif within the activation loop (Rodriguez *et al.*, 2010). Also in Sucrose non-fermenting 1-related Protein Kinase 1 (SnRK1), phosphorylation of the kinase domain is required for full activity (Emanuelle *et al.*, 2018). We propose that phosphorylation of HPCAL1 at S870 affects general kinase activity, while phosphorylation at S839 affects interaction with the substrate NRT2.1. Phosphorylation site T792 was predicted (InterPro, Mitchell *et al.*, 2019) within the activation loop of the kinase. However, under conditions used in our experiments, mutations of T792 did not affect the activity of HPCAL1. There are several kinases in which phosphorylation of the activation loop is not required for activation (Nolen *et al.*, 2004). Possibly, in HPCAL1, steric access to the activation loop and active center is regulated by (de) phosphorylation of S839 rather than by phosphorylation of

the activation loop itself. Recent structural analyses of kinase catalytic domains revealed that the activation loop requires N- and C-terminal structural anchors which correctly place the activation loop neighboring the ATP-binding site and catalytic domain (Nolen *et al.*, 2004). In HPCAL1, phosphorylation site S839 is located within a region that could serve as a C-terminal anchor for the activation loop. However, the precise role of different phosphorylation sites of the HPCA1/CARD1 protein family needs to be fully explored in further experiments.

In summary, serine residues S21 and S28 in the N-terminus of NRT2.1 activate nitrate influx in singly phosphorylated states. HPCAL1 was identified as the kinase phosphorylating and activating NRT2.1 at S21. The interaction of HPCAL1 with NRT2.1—which was favored when S28 was dephosphorylated—is further fine-tuned by phosphorylation within HPCAL1 at S839 and S870. Activity changes of NRT2.1 and effects on high-affinity nitrate transport activity are the final result.

Supplementary data

The following supplementary data are available at *JXB* online.

Fig. S1. Experimental datasets used in this study.

Fig, S2. Best spectra of NRT2.1 phosphopeptides directly exported from MaxQuant.

Fig, S3. Representative images of the interaction of NRT2.1 with NAR2.1.

Fig, S4. Workflow of identification of protein kinases which might phosphorylate NRT2.1.

Fig. S5. Best spectra of kinase HPCAL1 phosphopeptides directly exported from MaxQuant.

Fig. S6. Representative images of the interaction of ratiometric bimolecular fluorescence assays.

Fig. S7. SDS–PAGE gel detection after immobilized metal affinity chromatography (IMAC) purification of the intracellular domain of AT5G49760, AT5G49770, and AT5G49780.

Fig. S8. Protein abundances under conditions of nitrate uptake for NRT2.1, NAR2.1, and kinase HPCAL1.

Fig. S9. Doubly phosphorylated peptide of NRT2.1 covering sites S21 and S28.

Fig. S10. Nitrate influx by NRT2.1 with double phosphorylation site mutations at S21 and S28 at 4 h of induction by 1 mM nitrate.

Fig. S11. Close homologs of AT5G49770. The proteins AT5G49760 and AT5G49780 are closely related to the candidate kinase AT5G49770.

Table S1: List of primers used.

Table S2. Summary of identified phosphopeptides from the joint analysis of the nitrate deprivation experiment (Menz *et al.*, 2016) and nitrate starvation–resupply experiment with 0.2 mM and 5 mM nitrate resupply.

Table S3. Correlation network of NRT2.1 N-terminal phosphorylation sites with phosphorylation sites of different kinases under nitrogen deprivation (Menz *et al.*, 2016) and nitrate resupply with 0.2 mM and 5 mM nitrate.

Acknowledgements

Author contributions

ZL: performing the majority of experiments, developing the kinase–substrate network screen, and contributing to writing; XNW, performing rBiFC experiments; AJ, VC, MA, and BN: performing nitrate uptake and qPCR experiments; TS: performing nitrate uptake experiments on double mutants and contributing to writing; LL: data analysis and contributing to writing; WXS: data analysis, figure design, and writing.

Conflict of interest

The authors declare no conflict of interest.

Funding

Data availability

The raw MS data from this study were deposited at the ProteomeXchange Consortium (http://proteomecentral.proteomexchange.org) via the PRIDE partner repository with the identifier PXD015390 for the nitrate starvation dataset, and PXD014146 for the nitrate resupply dataset. Supplementary Tables S2 and S3 include the network raw data and phosphoproteome list.

References

Arif A, Jia J, Willard B, Li X, Fox PL. 2018. Multisite phosphorylation of S6K1 directs a kinase phospho-code that determines substrate selection. Molecular Cell **73**, 446–457.

Caesar K, Elgass K, Chen Z, Huppenberger P, Witthöft J, Schleifenbaum F, Blatt MR, Oecking C, Harter K. 2011. A fast brassinolide-regulated response pathway in the plasma membrane of *Arabidopsis thaliana*. The Plant Journal **66**, 528–540.

Camanes G, Bellmunt E, Garcia-Andrade J, Garcia-Agustin P, Cerezo M. 2012. Reciprocal regulation between AtNRT21 and AtAMT11 expression and the kinetics of NH_4^+ and NO_3^- influxes. Journal of Plant Physiology **169**, 268–274.

Cerezo M, Tillard P, Filleur S, Munos S, Daniel-Vedele F, Gojon A. 2001. Major alterations of the regulation of root NO_3^- uptake are associated with the mutation of Nrt21 and Nrt22 genes in Arabidopsis. Plant Physiology **127**, 262–271.

Cox J, Hein MY, Luber CA, Paron I, Nagaraj N, Mann M. 2014. Accurate proteome-wide label-free quantification by delayed normalization and maximal peptide ratio extraction, termed MaxLFQ. Molecular & Cellular Proteomics **13**, 2513–2526.

Cox J, Mann M. 2008. MaxQuant enables high peptide identification rates, individualized ppb-range mass accuracies and proteome-wide protein quantification. Nature Biotechnology **26**, 1367–1372.

Czechowski T, Bari RP, Stitt M, Scheible WR, Udvardi MK. 2004. Real-time RT–PCR profiling of over 1400 Arabidopsis transcription factors: unprecedented sensitivity revals novel root- and shoot-specific genes. The Plant Journal **38**, 366–379.

Emanuelle S, Doblin MS, Gooley PR, Gentry MS. 2018. The UBA domain of SnRK1 promotes activation and maintains catalytic activity. Biochemical and Biophysical Research Communications **497**, 127–132.

Engelsberger WR, Schulze WX. 2012. Nitrate and ammonium lead to distinct global dynamic phosphorylation patterns when resupplied to nitrogen starved Arabidopsis seedlings. The Plant Journal **69**, 978–995.

Franceschini A, Szklarczyk D, Frankild S, *et al*. 2013. STRING v91: protein–protein interaction networks, with increased coverage and integration. Nucleic Acids Research **41**, D808–D815.

Fuglsang AT, Borch J, Bych K, Jahn TP, Roepstorff P, Palmgren MG. 2003. The binding site for regulatory 14-3-3 protein in plant plasma membrane H+-ATPase: involvement of a region promoting phosphorylation-independent interaction in addition to the phosphorylation-dependent C-terminal end. Journal of Biological Chemistry **278**, 42266–42272.

Fuglsang AT, Kristensen A, Cuin T, *et al*. 2014. Receptor kinase mediated control of primary active proton pumping at the plasma membrane. The Plant Journal **80**, 951–964.

Gansel X, Muños S, Tillard P, Gojon A. 2001. Differential regulation of the NO_3 and NH_4 transporter genes AtNrt21 and AtAmt11 in Arabidopsis: relation with long-distance and local controls by N status of the plant. The Plant Journal **26**, 143–155.

Gilbert M, Li Z, Wu XN, Rohr L, Gombos S, Harter K, Schulze WX. 2021. Comparison of path-based centrality measures in protein–protein interaction networks revealed proteins with phenotypic relevance during adaptation to changing nitrogen environments. Journal of Proteomics **235**, 104114.

Gilbert M, Schulze WX. 2019. Global identification of protein complexes within the membrane proteome of Arabidopsis roots using a SEC-MS approach. Journal of Proteome Research **18**, 107–119.

Girin T, El-Kafafi -S, Widiez T, Erban A, Hubberten HM, Kopka J, Höfgen R, Gojon A, Lepetit M. 2010. Identification of Arabidopsis mutants impaired in the systemic regulation of root nitrate uptake by the nitrogen status of the plant. Plant Physiology **153**, 1250–1260.

Girin T, Lejay L, Wirth J, Widiez T, Palenchar PM, Nazoa P, Touraine B, Gojon A, Lepetit M. 2007. Identification of a 150bp cis-acting element of the AtNRT21 promoter involved in the regulation of gene expression by the N and C status of the plant. Plant, Cell & Environment **30**, 1366–1380.

Grefen C, Blatt MR. 2012. A 2in1 cloning system enables ratiometric bimolecular fluorescence complementation (rBiFC). Biotechniques **53**, 311–314.

Guo FQ, Wang R, Chen M, Crawford NM. 2001. The Arabidopsis dual-affinity nitrate transporter gene AtNRT11 (CHL1) is activated and functions in nascent organ development during vegetative and reproductive growth. The Plant Cell **13**, 1761–1777.

Haruta M, Gray WM, Sussman MR. 2015. Regulation of the plasma membrane proton pump (H-ATPase) by phosphorylation. Current Opinion in Plant Biology **28**, 68–75.

Haruta M, Monshausen G, Gilroy S, Sussman MR. 2008. A cytoplasmic Ca2+ functional assay for identifying and purifying endogenous cell signaling peptides in Arabidopsis seedlings: identification of AtRALF1 peptide. Biochemistry **47**, 6311–6321.

Ho C-H, Lin SH, Hu HC, Tsay YF. 2009. CHL1 functions as a nitrate sensor in plants. Cell **138**, 1184–1194.

Huala E, Dickerman AW, Garcia-Hernandez M, *et al*. 2001. The Arabidopsis information resource (TAIR): a comprehensive database and web-based information retrieval, analysis, and visualization system for a model plant. Nucleic Acids Research **29**, 102–105.

Jacquot A, Chaput V, Mauries A, *et al*. 2020. NRT21 phosphorylation prevents root high affinity nitrate uptake activity in *Arabidopsis thaliana*. New Phytologist **228**, 1038–1054.

Kiba T, Feria-Bourrellier A-B, Lafouge F, *et al*. 2012. The Arabidopsis nitrate transporter NRT24 plays a double role in roots and shoots of nitrogen-starved plants. The Plant Cell **24**, 245–258.

Krapp A, David LC, Chardin C, Girin T, Marmagne A, Leprince AS, Chaillou S, Ferrario-Mery S, Meyer C, Daniel-Vedele F. 2014. Nitrate transport and signalling in Arabidopsis. Journal of Experimental Botany **65**, 789–798.

Krouk G, Crawford NM, Coruzzi GM, Tsay YF. 2010. Nitrate signaling: adaptation to fluctuating environments. Current Opinion in Plant Biology **13**, 266–273.

Laohavisit A, Wakatake T, Ishihama N, Mulvey H, Takizawa K, Suzuki T, Shirasu K. 2020. Quinone perception in plants via leucine-rich-repeat receptor-like kinases. Nature **587**, 92–97.

Laugier E, Bouguyon E, Mauriès A, Tillard P, Gojon A, Lejay L. 2012. Regulation of high-affinity nitrate uptake in roots of Arabidopsis depends predominantly on posttranscriptional control of the NRT21/NAR21 transport system. Plant Physiology **158**, 1067–1078.

Lejay L, Gansel X, Cerezo M, Tillard P, Müller C, Krapp A, von Wirén N, Daniel-Vedele F, Gojon A. 2003. Regulation of root ion transporters by photosynthesis: functional importance and relation with hexokinase. The Plant Cell **15**, 2218–2232.

Lejay L, Tillard P, Domingo-Olive F, Lepetit M, Olive FD, Filleur S, Daniel-Vedele F, Gojon A. 1999. Molecular and functional regulation of two NO_3^- uptake systems by N- and C-status of Arabidopsis plants. The Plant Journal **18**, 509–519.

Leran S, Varala K, Boyer JC, *et al*. 2014. A unified nomenclature of NITRATE TRANSPORTER 1/PEPTIDE TRANSPORTER family members in plants. Trends in Plant Science **19**, 5–9.

Li G, Tillard P, Gojon A, Maurel C. 2016. Dual regulation of root hydraulic conductivity and plasma membrane aquaporins by plant nitrate accumulation and high-affinity nitrate transporter NRT21. Plant and Cell Physiology **57**, 733–742.

Liu KH, Huang CY, Tsay YF. 1999. CHL1 is a dual-affinity nitrate transporter of Arabidopsis involved in multiple phases of nitrate uptake. The Plant Cell **11**, 865–874.

Liu KH, Tsay YF. 2003. Switching between the two action modes of the dual-affinity nitrate transporter CHL1 by phosphorylation. The EMBO Journal **22**, 1005–1013.

Menz J, Li Z, Schulze W, Ludewig U. 2016. Early nitrogen-deprivation responses in Arabidopsis roots reveal distinct differences on transcriptome and (phospho-) proteome levels between nitrate and ammonium nutrition. The Plant Journal **88**, 717–734.

Mitchell AL, Attwood TK, Babbitt PC, *et al*. 2019. InterPro in 2019: improving coverage, classification and access to protein sequence annotations. Nucleic Acids Research **47**, D351–D360.

Nolen B, Taylor S, Ghosh G. 2004. Regulation of protein kinases; controlling activity through activation segment conformation. Molecular Cell **15**, 661–675.

Ohkubo Y, Kuwata K, Matsubayashi Y. 2021. A type 2C protein phosphatase activates high-affinity nitrate uptake by dephosphorylating NRT21. Nature Plants **7**, 310–316.

Orsel M, Chopin F, Leleu O, Smith SJ, Krapp A, Daniel-Vedele F, Miller AJ. 2006. Characterization of a two-component high-affinity nitrate uptake system in Arabidopsis physiology and protein–protein interaction. Plant Physiology **142**, 1304–1317.

Orsel M, Chopin F, Leleu O, Smith SJ, Krapp A, Vedele FD, Miller AJ. 2007. Nitrate signaling and the two component high affinity uptake systems in Arabidopsis. Plant Signaling & Behaviour **2**, 260–262.

Parker JL, Newstead S. 2014. Molecular basis of nitrate uptake by the plant nitrate transporter NRT11. Nature **507**, 68–72.

Perraki A, DeFalco TA, Derbyshire P, *et al*. 2018. Phosphocode-dependent functional dichotomy of a common co-receptor in plant signaling. Nature **561**, 248–252.

Pertl H, Himly M, Gehwolf R, Kriechbaumer R, Strasser D, Michalke W, Richter K, Ferreira F, Obermeyer G. 2001. Molecular and physiological characterisation of a 14-3-3 protein from lily pollen grains regulating the activity of the plasma membrane H+ ATPase during pollen grain germination and tube growth. Planta **213**, 132–141.

Rodriguez MC, Petersen M, Mundy J. 2010. Mitogen-activated protein kinase signaling in plants. Annual Review of Plant Biology **61**, 621–649.

Rudashevskaya EL, Ye J, Jensen ON, Fuglsang AT, Palmgren MG. 2012. Phosphosite mapping of P-type plasma membrane H+-ATPase in homologous and heterologous environments. Journal of Biological Chemistry **287**, 4904–4913.

Schindelin J, Arganda-Carreras I, Frise E, *et al*. 2012. Fiji: an open-source platform for biological-image analysis. Nature Methods **9**, 676–682.

Schultz J, Milpertz F, Bork P, Ponting CP. 1998. SMART, a simple modular architecture research tool: identification of signaling domains. Proceedings of the National Academy of Sciences, USA **95**, 5857–5864.

Tan YZ, Keon KA, Abdelaziz R, Imming P, Schulze W, Schumacher K, Rubinstein JL. 2022. Structure of V-ATPase from citrus fruit. Structure **30**, 1403–1410.

Tanz SK, Castleden I, Hooper CM, Vacher M, Small I, Millar HA. 2013. SUBA3: a database for integrating experimentation and prediction to define the SUBcellular location of proteins in Arabidopsis. Nucleic Acids Research **41**, D1185–D1191.

Thimm O, Bläsing O, Gibon Y, Nagel A, Meyer S, Kruger P, Selbig J, Muller LA, Rhee SY, Stitt M. 2004. MAPMAN: a user-driven tool to display genomics data sets onto diagrams of metabolic pathways and other biological processes. The Plant Journal **37**, 914–939.

Tyanova S, Temu T, Sinitcyn P, Carlson A, Hein MY, Geiger T, Mann M, Cox J. 2016. The Perseus computational platform for comprehensive analysis of (prote)omics data. Nature Methods **13**, 731–740.

Wang X, Bian Y, Cheng K, Gu L-F, Ye M, Zou H, He J-X. 2013. A large-scale protein phosphorylation analysis reveals novel phosphorylation motifs and phosphoregulatory networks in Arabidopsis. Journal of Proteomics **14**, 486–498.

Wang YY, Hsu PK, Tsay YF. 2012. Uptake, allocation and signaling of nitrate. Trends in Plant Science **17**, 458–467.

Wingenter K, Trentmann O, Winschuh I, Hörmiller II, Heyer AG, Reinders J, Schulz A, Geiger D, Hedrich R, Neuhaus HE. 2011. A member of the mitogen-activated protein 3-kinase family is involved in the regulation of plant vacuolar glucose uptake. The Plant Journal **68**, 890–900.

Winter D, Vinegar B, Nahal H, Ammar R, Wilson GV, Provart NJ. 2007. An 'electronic fluorescent pictograph' browser for exploring and analyzing large-scale biological data sets. PLoS One **2**, e718.

Wirth J, Chopin F, Santoni V, Viennois G, Tillard P, Krapp A, Lejay L, Daniel-Vedele F, Gojon A. 2007. Regulation of root nitrate uptake at the NRT21 protein level in *Arabidopsis thaliana*. Journal of Biological Chemistry **282**, 23541–23552.

Wu F, Chi Y, Jiang Z, *et al*. 2020. Hydrogen peroxide sensor HPCA1 is an LRR receptor kinase in Arabidopsis. Nature **578**, 577–581.

Wu X, Liu T, Zhang Y, Duan F, Neuhauser B, Ludewig U, Schulze WX, Yuan L. 2019. Ammonium and nitrate regulate NH_4^+ uptake activity of Arabidopsis ammonium transporter AtAMT1;3 via phosphorylation at multiple C-terminal sites. Journal of Experimental Botany **70**, 4919–4930.

Wu XN, Chu L, Xi L, Pertl-Obermeyer H, Li Z, Sklodowski K, Sanchez-Rodriguez C, Obermeyer G, Schulze WX. 2019. Sucrose-induced receptor kinase 1 is modulated by an interacting kinase with short extracellular domain. Molecular & Cellular Proteomics **18**, 1556–1571.

Wu XN, Schulze WX. 2015. Kinase activity and specificity assay using synthetic peptides. Methods in Molecular Biology **1306**, 97–104.

Wu XN, Xi L, Pertl-Obermeyer H, Li Z, Chu LC, Schulze WX. 2017. Highly efficient single-step enrichment of low abundance phosphopeptides from plant membrane preparations. Frontiers in Plant Science **8**, 1673.

Yong Z, Kotur Z, Glass AD. 2010. Characterization of an intact two-component high-affinity nitrate transporter from Arabidopsis roots. The Plant Journal **63**, 739–748.

Zauber H, Schulze WX. 2012. Proteomics wants cRacker: automated standardized data analysis of LC/MS derived proteomic data. Journal of Proteome Research **11**, 5548–5555.

Zou X, Liu M, Wu W, Wang Y. 2019. Phosphorylaiton at Ser28 stabilizes the Arabidopsis nitrate transporter NRT21 in response to nitrate limitation. Journal of Integrative Plant Biology **62**, 865–876.

Zulawski M, Schulze WX. 2015. The plant kinome. Methods in Molecular Biology **1306**, 1–23.